

A high light-yield neutron scintillator based on Ce^{3+}-doped lithium glass

Rui-Qiang Song(宋瑞强), Chuang Liu(刘闯), Yi-Yang Long(龙逸洋), Ji-Feng Han(韩纪锋), Jing Ren(任晶), and Sen Qian(钱森)

Citation: Chin. Phys. B, 2025, 34 (**5**): 050703. DOI: 10.1088/1674-1056/adb94b
Journal homepage: http://cpb.iphy.ac.cn; http://iopscience.iop.org/cpb

What follows is a list of articles you may be interested in

Suppression of the vapor cell temperature error in a spin-exchange relaxation-free comagnetometer

Jia-Li Liu(刘佳丽), Li-Wei Jiang(姜丽伟), Chi Fang(方驰), Xin Zhao(赵鑫), and Yuan-Qiang Chen(陈远强)
Chin. Phys. B, 2024, 33 (**12**): 120701. DOI: 10.1088/1674-1056/ad84ce

Determination of liquid viscosity based on dual-frequency-band particle tracking

Lihua Yan(闫丽华), Boyin Xue(薛博引), Yuanji Li(李渊骥), Jinxia Feng(冯晋霞), Xingkang Wu(武兴康), and Kuanshou Zhang(张宽收)
Chin. Phys. B, 2024, 33 (**9**): 090701. DOI: 10.1088/1674-1056/ad597e

Deep learning-assisted common temperature measurement based on visible light imaging

Jia-Yi Zhu(朱佳仪), Zhi-Min He(何志民), Cheng Huang(黄成), Jun Zeng(曾峻), Hui-Chuan Lin(林惠川), Fu-Chang Chen(陈福昌), Chao-Qun Yu(余超群), Yan Li(李燕), Yong-Tao Zhang(张永涛), Huan-Ting Chen(陈焕庭), and Ji-Xiong Pu(蒲继雄)
Chin. Phys. B, 2024, 33 (**8**): 080701. DOI: 10.1088/1674-1056/ad4cd9

Performance optimization of a SERF atomic magnetometer based on flat-top light beam

Ziqi Yuan(袁子琪), Junjian Tang(唐钧剑), Shudong Lin(林树东), and Yueyang Zhai(翟跃阳)
Chin. Phys. B, 2024, 33 (**6**): 060703. DOI: 10.1088/1674-1056/ad401b

A stopping layer concept to improve the spatial resolution of gas-electron-multiplier neutron detector

Jianjin Zhou(周建晋), Jianrong Zhou(周健荣), Xiaojuan Zhou(周晓娟), Lin Zhu(朱林), Jianqing Yang(杨建清), Guian Yang(杨桂安), Yi Zhang(张毅), Baowei Ding(丁宝卫), Bitao Hu(胡碧涛), Zhijia Sun(孙志嘉), Limin Duan(段利敏), and Yuanbo Chen(陈元柏)
Chin. Phys. B, 2022, 31 (**5**): 050702. DOI: 10.1088/1674-1056/ac398e

---

A high light-yield neutron scintillator based on Ce^{3+}-doped lithium glass

Rui-Qiang Song(宋瑞强)[1,3,†], Chuang Liu(刘闯)[2,†], Yi-Yang Long(龙逸洋)[1], Ji-Feng Han(韩纪锋)[1,‡], Jing Ren(任晶)[2,§], and Sen Qian(钱森)[3,¶]

[1] *Key Laboratory of Radiation Physics and Technology of the Ministry of Education, Institute of Nuclear Science and Technology, Sichuan University, Chengdu* 610064, *China*

[2] *College of Physics and Optoelectronic Engineering, Harbin Engineering University, Harbin* 150001, *China*

[3] *Institute of High Energy Physics, Chinese Academy of Sciences, Beijing* 100049, *China*

(Received 30 December 2024; revised manuscript received 13 February 2025; accepted manuscript online 24 February 2025)

The development of low-cost and highly efficient thermal neutron detection materials to substitute the rare and expensive ^{3}He gas is important for applications requiring thermal neutron detection. Lithium-based glass (Li glass) is a promising candidate due to its simple fabrication process and low cost. This paper reports the optical properties and scintillation performance of a new Ce^{3+}-doped Li glass, whose luminescence efficiency is significantly enhanced with a light yield of about 4770 ph/MeV, which is about 54% of that of BGO crystal, and the energy resolution is 14.5% for 662 keV gamma rays. The Ce^{3+}-doped Li glass shows a high light yield of about 7058 ph/neutron, which is about 1.18 times that of the reference GS20 glass. The Ce^{3+}-doped Li glass exhibits stronger gamma ray suppression capability compared to GS20 glass samples. Further optimizing the Ce^{3+} concentration and ^{6}Li content is expected to achieve much superior neutron detection efficiency, positioning it as a promising alternative to ^{3}He gas for efficient thermal neutron detection.

Keywords: thermal neutron detection, neutron scintillator, Li glass, light yield

PACS: 07.07.Df, 28.20.Fc, 29.30.Hs, 29.40.Mc

DOI: 10.1088/1674-1056/adb94b **CSTR:** 32038.14.CPB.adb94b

1. Introduction

Thermal neutron detectors play an important role in applications such as nuclear safety, medicine, industrial neutron imaging and resource exploration. With the establishment of large scientific facilities and the development of nuclear science and technology,[1,2] the demand for thermal neutron detection is increasing. The shortage of ^{3}He gas has accelerated the development of high-performance alternative materials for neutron detection.[3] Doping certain neutron-sensitive nuclides into solid scintillation materials is an effective method for neutron detection, where high-energy secondary charged ions are generated upon neutron capture, and numerous optical photons are further generated in the scintillator through ionization of these secondary ions, which can be changed to electric signal through photon-electric devices.[4–7] The desired properties for scintillators used in neutron detection include high light yield, short decay time, non-hygroscopic nature, large neutron capture cross-section and good neutron/γ discrimination capability. In practice, ^{6}Li and ^{10}B are commonly incorporated into solid scintillators to achieve higher thermal neutron capture efficiency. Therefore, many scintillators containing ^{6}Li and ^{10}B have attracted extensive attention, including boron-containing plastic scintillators,[8] boron-containing glass scintillators,[9] lithium-containing crystal scintillators,[10] lithium-containing glass scintillators[11] and lithium-containing plastic scintillators.[12] Comparing boron and lithium-containing scintillators, ^{10}B(n, α)^{7}Li reaction has a higher thermal neutron capture cross-section ($\sim$ 3840 barns) than that of ^{6}Li(n, t)^{4}He reaction ($\sim$ 940 barns).[13,14] Although the thermal neutron reaction cross-section of ^{10}B is higher than that of ^{6}Li, the reaction Q-value of ^{10}B(n, α)^{7}Li is about 2.31 MeV, which is lower than the value of 4.78 MeV for ^{6}Li(n, t)^{4}He.[15] Therefore, lithium-containing scintillators can generate much larger neutron signals and are more suitable for thermal neutron detection. The plastic scintillators mainly consist of low-atomic-number ($Z_{\rm eff}$) nuclides, such as H and C, which are very efficient for high-energy neutron detection through elastic scattering, but the energy resolution is not good. There is a method to add ^{10}B to the plastic to make it sensitive to thermal neutrons, but the quenching effect is very heavy, and a neutron and gamma discrimination method is needed.[16]

There are many lithium-containing crystal scintillators, especially inorganic scintillators such as ZnS/LiF,[17] LiI:Eu^{2+},[18] $LiBaF_3$:Ce,[19] Cs_2LiYCl_6:Ce[20]

†These authors contributed equally to this work.

‡Corresponding author. E-mail: hanjf@scu.edu.cn

§Corresponding author. E-mail: ren.jing@hrbeu.edu.cn

¶Corresponding author. E-mail: qians@ihep.ac.cn

© 2025 Chinese Physical Society and IOP Publishing Ltd. All rights, including for text and data mining, AI training, and similar technologies, are reserved.

and $Cs_2LiLaBr_6$:Ce.[21] These crystal scintillators have better transparency, higher detection efficiency and better resolution. In addition, multi-mode detection of neutrons and gamma rays by pulse shape discrimination (PSD) is possible.[22,23] However, crystal scintillators are susceptible to moisture, making them difficult to use in extreme environments.[24] Crystals are typically grown using the Czochralski method, micro-pulling-down method, or the Bridgman method.[25,26] These growth processes are rigorous, costly, and it is difficult to process single-crystal scintillators to large sizes. Lithium-containing glass scintillators (Li glass) are inert and have high transparency, which ensures excellent stability and light output efficiency. Compared to crystal scintillators, glass is easy to process into any shape and size due to the non-salting nature of the melting process, offering significant advantages in large-size preparation and fiber optics preparation for radiation monitoring in various environments. Furthermore, glass is easily moldable, allowing continuous adjustment of the composition to facilitate the development of suitable scintillators. Currently, ^{6}Li-glass scintillators are widely used in thermal neutron detection and spectroscopy.[27,28]

The optical and scintillation properties of scintillation materials are predominantly governed by the selection of luminescent centers and substrates. Rare earth elements have garnered significant research interest owing to their exceptional chemical stability and outstanding luminescent properties. The rare earth element luminescent center of the 4f–5f transition exhibits enhanced stability in fluorescence performance, with a narrower emission band that remains impervious to external influences. Furthermore, the 4f–5d transition enables the generation of a wide range of fluorescence emissions, from ultraviolet to near-infrared light.[29] The ions commonly used as luminescent centers in glass scintillators are Ce^{3+} and Eu^{2+}. Compared to Eu^{2+} ions, the decay time of the Ce^{3+} emission center is on the order of ns, while that of Eu^{2+} is $\sim$ µs.[30] The luminescence generated by Ce^{3+} as the luminescent center of the glass scintillator has higher light output, good energy resolution, faster decay time, and is currently the best activator in scintillating glass.[31] In addition, the efficient halides can provide an ideal low-phonon-energy halide environment for the activator, which maintains the benefits of high transparency of oxide glass while improving chemical durability and thermal stability.[32] However, due to the amorphous nature of glasses, carriers tend to be trapped by many defect sites in the amorphous matrix, resulting in relatively low light yield ($<$ 1000 ph/MeV) and poor optical properties for most glasses. Therefore, only a small number of commercially available lithium glasses exhibit high light yield, e.g., Ce^{3+} doped lithium alumino-silicate glass (GS20), with a gamma light yield of $\sim$ 4000 ph/MeV and a neutron light yield of $\sim$ 6000 ph/MeV, are primarily used for thermal neutron detection.[33,34]

With the rapid development of neutron detection technology, neutron detection materials face increasingly stringent requirements in terms of detection efficiency, energy resolution and neutron/γ discrimination. It has been reported that oxide glasses offer excellent stability, while fluoride crystals have the advantage of low phonon energy.[35] Sr_2GdF_7:Tb^{3+} glass-ceramics combine the advantages of oxide glasses and fluoride crystals to exhibit strong optical properties and high light output, with XEL-measured intensities up to 194% of that of BGO.[35] This research study has made significant progress in improving the light output of glass scintillators. To improve the light yield of glass scintillators, we have combined the advantages of oxides and fluorides to study the Li glass performance at high Ce^{3+} content. The incorporation of ^{6}Li in the glass matrix increases the sensitivity to thermal neutrons. This study aims to develop low-cost Li glass with high light yield, which is expected to be used in large-area neutron detection and neutron imaging.

2. Experimental equipment and methods

The high Ce^{3+}-doped Li glass in this study was synthesized using a conventional high-temperature melt-quenching technique. High-purity (4N) raw materials from Aladdin Co. were precisely weighed according to the target glass composition. The starting materials were homogenized using a planetary ball mill (with ZrO_2 grinding balls), dried and sieved for subsequent use. Prior to melting, the mixed powder was loaded into an alumina crucible and pre-calcined in a muffle furnace at 800 °C. The pre-calcined product was then reground in the planetary ball mill to ensure homogeneity. The homogenized powder was transferred back into the alumina crucible and melted in a tube furnace at 1400 °C under a continuous gas flow (H_2 and N_2 mixture) to reduce oxygen, which is used to facilitate the reduction of Ce^{4+} to Ce^{3+}. The molten glass was rapidly quenched into a preheated stainless-steel mold at 500 °C. The solidified glass was immediately transferred to an annealing furnace, where it underwent stress-relief treatment for several hours before cooling down. Finally, the annealed glasses were subsequently cut into specimens and polished to optical-grade surface quality for optical transmission, luminescence, and scintillation performance evaluations. The Ce^{3+}-doped glass was cut into cubes of $5 \times 5 \times 5$ mm^3 size, and $25 \times 25 \times 5$ mm^3 size, as shown in Fig. 1. The Ce^{3+}-doped Li glass shows enough transparency to see the pattern on the backside. The Ce^{3+}-doped Li glass shows intense blue light under UV excitation, as shown in Fig. 1(b).

A UV spectrophotometer and a spectrograph were utilized for spectroscopy measurements. The scintillator was enclosed on five sides with Teflon film, while silicon grease served as the optical coupling agent. The study employed a

Hamamatsu S13360-6025CS Silicon Photomultiplier (SiPM), which has an effective area of 6×6 mm^2 and a pixel size of 25 μm. It was operated using the Hamamatsu C12332-01 driver circuit. For detector calibration, gamma-ray spectra were measured using a ^{137}Cs gamma-ray source. To evaluate the neutron response of the Ce^{3+}-doped Li glass, an Am–Be neutron source with an activity of 0.51 MBq was used. Signals from the SiPM were recorded using a high-speed digitizer (DT5751), and the data were subsequently transmitted to a computer via a high-speed communication line for storage. A comparative test was conducted using commercial BGO and GS20 glass scintillators under identical testing conditions to evaluate the performance of the novel Ce^{3+}-doped Li glass in gamma and neutron detection.

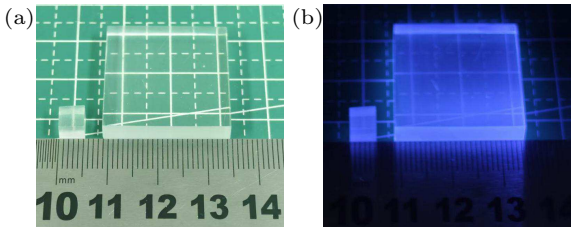


Fig. 1. Two polished 5 mm thick Ce^{3+}-doped Li glass samples (a) and their images under UV illumination (b).

3. Measurements with Ce^{3+}-doped Li glass

3.1. Spectroscopy measurements

Transmittance spectra of the Ce^{3+}-doped Li glass are shown in Fig. 2. This glass has a high transmittance exceeding 80% in the range of 390–800 nm. The optical transmission performance in the blue and near-infrared wavelength bands is good, enabling coupling with photon-electric devices.

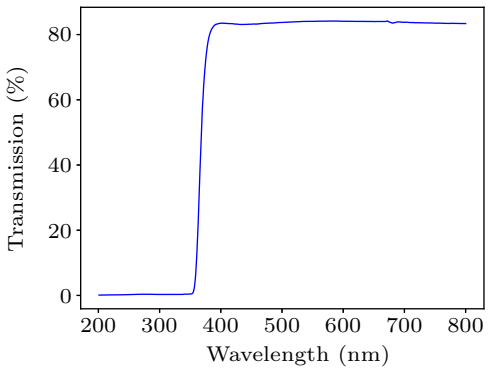


Fig. 2. Transmittance curves of Ce^{3+}-doped Li glass.

The normalized photoluminescence (PL) and photoluminescence excitation (PLE) spectra of the high Ce^{3+}-doped Li glass, are shown in Fig. 3. The PL spectrum shows that the glass scintillator has a broadband emission in the range of 360–600 nm. The emission peak at about 400 nm under the 354 nm excitation peak is mainly attributed to the transition in the 5d–4f bands of Ce^{3+} ions.[36] A Stokes shift of 47 nm of the PL and PLE spectra indicates a relatively weak self-absorption in the glass, which facilitates the transport of scintillation light.

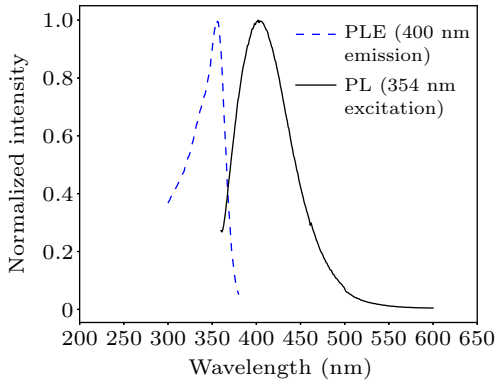


Fig. 3. PL and PLE spectra of the Ce^{3+}-doped Li glass.

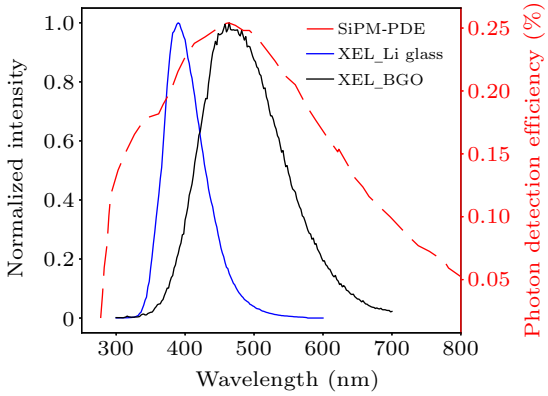


Fig. 4. X-ray excited luminescence (XEL) emission spectra of Ce^{3+}-doped Li glass and BGO crystal, as well as the photon detection efficiency curve of SiPM.

The light yield of scintillators is converted by the photon detection efficiencies (PDE) of SiPM and the XEL emission spectrum of the scintillator.[37] The x-ray excitation emission (XEL) spectra of the Ce^{3+}-doped Li glass and a commercial BGO standard sample with the same size of $5 \times 5 \times 5$ mm^3 are shown in Fig. 4. The Ce^{3+}-doped Li glass exhibits broad emission in the range of 350–500 nm under x-ray excitation. The emission peak is located at about 390 nm, and the XEL spectrum of Ce^{3+}-doped Li glass is very similar to that of GS20 glass.[11] The emission peak of the BGO scintillator is located at about 470 nm. It is important to select a photodetector that can be adapted to the glass scintillator for light collection. The spectral response of SiPM is from 270–900 nm and the peak-sensitive wavelength is 450 nm. The photon detection efficiency curve (data from the Hamamatsu product brochure) is shown as a red dotted line in Fig. 4. The formula for calculating the light yield is as follows:[37]

$$\text{Light_Yield} = \frac{M_{\text{E}} \times 1000\ \text{keV}}{S \times \varepsilon_{\text{PDE}} \times E\ \text{keV}}, \tag{1}$$

where M_{E} is the channel number of the full-energy peaks, S is the single photoelectron channel number, ε_{PDE} is the weighted

photon detection efficiency (PDE) of the SiPM and E is the energy of the γ-ray source. The unit of light yield is photons per MeV, indicating the number of photons that can be produced when 1 MeV gamma-ray is absorbed by the scintillator.

3.2. Gamma-ray measurements

The commercial GS20 standard sample and BGO crystal were used to compare the light yield of Ce^{3+}-doped Li glass. These three scintillators were coupled to the same SiPM for measurements with a ^{137}Cs gamma-ray source. The gamma-ray spectra of Ce^{3+}-doped Li glass, GS20 glass and BGO crystal are shown in Fig. 5. The full energy peak of the high-Ce^{3+}-doped Li glass is not prominent when compared to the Compton plateau due to the low density (2.47 g/cm^3) and small size, but the complete full peaks can be observed. The channel numbers were obtained by Gaussian fitting of the full-energy peaks for ^{137}Cs at 662 keV. By fitting the full energy peaks, the energy resolution ($\Delta E/E$) of BGO crystals is about 10.0%, while that of Ce^{3+}-doped Li glass is about 14.5%. The channel numbers of the full-energy peak for the Ce^{3+}-doped Li glass and the BGO crystal are 35430 and 68670, respectively. Therefore, the light yield of the BGO crystal is about 8843 ph/MeV, and the light yield of the Ce^{3+}-doped Li glass is about 4770 ph/MeV. The light yield of the Ce^{3+}-doped Li glass is equivalent to about 54% of the BGO crystal.

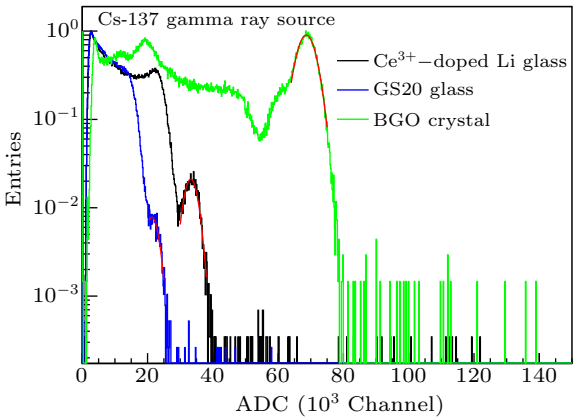


Fig. 5. Gamma-ray spectra of Ce^{3+}-doped Li glass, GS20 glass and BGO crystal for ^{137}Cs source.

Due to the low density (2.5 g/cm^3) and small thickness (only 1 mm) of the GS20 glass sample, the full-energy peak is unclear. By Gaussian fitting of the full-energy peak on a logarithmic scale, the energy resolution is about 26.0%, with the center channel number of the full-energy peak at 20853. Therefore, the light yield of the GS20 glass sample is about 2807 ph/MeV. The measured light yield of the GS20 glass sample was smaller than the reported value of 4000 ph/MeV,[34] possibly because the thickness is too small and there are drawbacks inside the tested sample. The light yield of the Ce^{3+}-doped Li glass is equivalent to about 170% of the tested GS20 glass sample and about 119% of the reported GS20 glass. The measurement uncertainty of the light yield mainly comes from the accuracy of the instrument as well as the measurement. After several measurements, the uncertainty of the light yield is found to be around 5%.

3.3. Neutron measurements

Since ^{6}Li has a high thermal neutron capture cross-section ($\sim$ 960 barns), the Ce^{3+}-doped Li glass has good thermal neutron detection capability. The neutron response of the Ce^{3+}-doped Li glass and GS20 glass sample were compared under an Am–Be neutron source. Neutrons were moderated to thermal neutrons by an 8 cm thick layer of paraffin in front of the Am–Be source with an activity of 0.51 MBq. To shield the high-energy gamma rays generated by the Am–Be neutron source, a 5 cm thick lead brick was placed behind the moderator. A fast PMT (XP2020 PMT) is used to measure the decay time of the Ce^{3+}-doped Li glass. The neutron-averaged waveform was obtained by 800 pulses, as shown in Fig. 6.

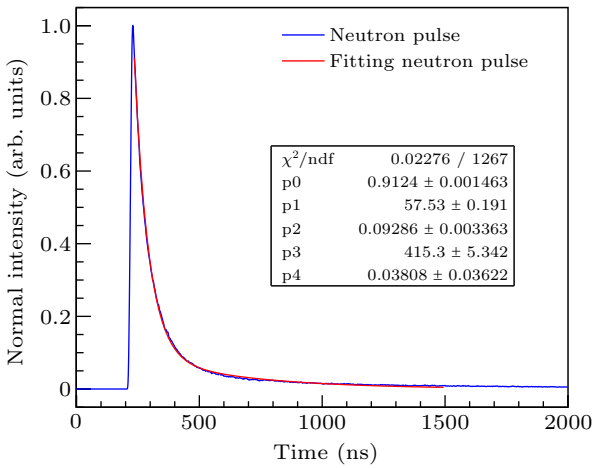


Fig. 6. Average pulse waveform of Ce^{3+}-doped Li glass.

The decay curves were fitted with a double exponential function. The fitting function is expressed as

$$y = A_1 \exp\left(-\frac{x}{t_1}\right) + A_2 \exp\left(-\frac{x}{t_2}\right) + y_0. \tag{2}$$

Based on Eq. (2), the scintillation decay time is divided into two main components; a fast component and a slow component. The fast component decay time is about 58 ns (57.86%) and the slow component decay time is about 415 ns (42.14%).

The neutron spectra of the Ce^{3+}-doped Li glass and GS20 glass sample under the Am–Be neutron source are shown in Fig. 7. Two peaks corresponding to thermal neutrons are clearly observed. The Gaussian fitting of the thermal neutron peaks of the Ce^{3+}-doped Li glass and the GS20 glass sample indicated channel numbers 79200 and 54040, respectively. The relative width (FWHM/mean) of the thermal neutron peak for the Ce^{3+}-doped Li glass is about 10.5%, which is better

than the 24.0% of the GS20 sample. It is worth noting that natural lithium with ^{6}Li enrichment of 7.5% is used in this work, which means the neutron detection efficiency will be greatly enhanced if 95% enriched ^{6}Li is used as that of the GS20 glass sample.

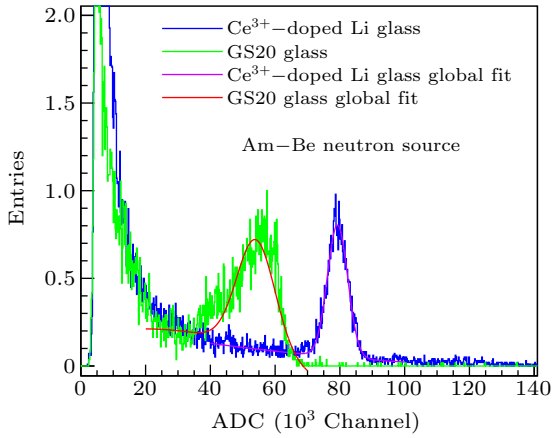


Fig. 7. Energy spectra for Ce^{3+}-doped Li glass and the GS20 glass sample under Am–Be neutron source.

The neutron light yield of Ce^{3+}-doped Li glass is about 7058 ph/neutron, and the neutron light yield of the GS20 glass sample is about 4816 ph/neutron. The measured light yield of the GS20 glass sample was smaller than the reported value of 6000 ph/neutron.[34] The neutron light yield of Ce^{3+}-doped Li glass is equivalent to about 147% of the tested GS20 glass sample and about 118% of the reported GS20 glass. In addition, the gamma light yield of the Ce^{3+}-doped Li glass is 4770 ph/MeV, which is higher than that of 4000 ph/MeV for the GS20 glass sample.[33]

In the glass matrix, high-energy gamma rays or charged particles induce ionization within the scintillator material. The energy of the liberated electrons is transferred to activator ions (e.g., Ce^{3+}), which will excite their valence electrons to higher energy states. Subsequent radiative transitions of these electrons back to the ground state result in photon emission at characteristic wavelengths. For the Ce^{3+}-doped Li glass, the excitation can migrate to Ce^{3+} ions and render recombination of the Ce^{3+} ions, resulting in further light emission. Thus, enhancing energy transfer from electron–hole excitation to Ce^{3+} ions is the key issue to increasing light yield. From the perspective of neutron capture, a higher content of ^{6}Li is preferred to increase the neutron reaction possibility. However, an excessive content of Li^+ will increase the difficulty of converting Ce^{4+} ions to Ce^{3+} ions, and a high content of Li^+ will render the existence of non-bridging oxygen energy trapping centers.[38,39] Therefore, the concentration of Li and Ce in the glass matrix must be carefully balanced during melting. A 'H_2/N_2' mixed gas is used to create a low oxygen environment to ensure that most of the scintillating ions in the glass matrix exist as Ce^{3+}. In addition, Al_2O_3 is added to the Li glass melting process to reduce the concentration of non-bridging oxygen and decrease the melting temperature, which is beneficial for shaping the Li glass. After melting and shaping, the glass is transferred to an annealing furnace to eliminate internal stress. Using the above mentioned methods, the light yield of Ce^{3+}-doped Li glass can be effectively improved.

When the neutrons are captured by the scintillator, the ^{6}Li(n, t)α reaction produces high-energy α and tritium particles. These high-energy particles interact with atoms or molecules in the scintillator to produce quenching effects, resulting in varying degrees of energy loss from the particles.[40] The quenching factor (q) represents the ratio of the detected energy relative to the deposited energy, the larger q indicates a smaller energy loss of the incident particle. The q is defined as[41]

$$q = \frac{E_{\text{eq.}}}{E_{\text{N}} + Q}, \tag{3}$$

where $E_{\text{eq.}}$ is the measured equivalent electron-volt energy, E_{N} is the incident neutron energy and Q is the Q-value of the reaction. The E_{N} is negligible for thermal neutrons and the Q-value is 4.78 MeV. The neutron energy spectra were calibrated by gamma equivalent energy to obtain the neutron energy corresponding to the thermal neutron peaks. For Ce^{3+}-doped Li glass and the GS20 glass sample, the $E_{\text{eq.}}$ was calculated to be 1.48 MeV and 1.71 MeV, respectively. The resulting quenching factors of the Ce^{3+}-doped Li glass and the GS20 sample are 0.31 and 0.36, respectively, for the ^{6}Li(n, t)α reaction. The quenching factor (q) of the Ce^{3+}-doped Li glass is slightly lower than that of the GS20 glass sample.

For the Ce^{3+}-doped Li glass and the GS20 glass sample, the pulse shapes of neutrons and gamma rays are similar, making it difficult to discriminate using the pulse shape discrimination method. However, conventional pulse height analysis or pulse integration methods are used because the neutron signals are similar and much larger, forming a neutron peak on the high-energy side, while the gamma rays are mainly distributed on the low energy side due to the low density of the Li glass. The ratio of gamma rays that are located within the neutron peak can be used to represent the neutron/γ discrimination performance. The gamma-ray spectrum can be deduced by fitting the energy spectrum without the neutron peak, and the components of gamma rays within the neutron peak can be calculated. Therefore, by fitting the spectrum of the neutron peak and the gamma ray background, the quantitative evaluation of the gamma-ray suppression capabilities of Ce^{3+}-doped Li glass and the GS20 glass sample is acquired. Comparing the neutron energy spectra of the two glass scintillators reveals differences in the proportion of gamma rays at the neutron peaks, which can lead to an increased misclassification rate for neutrons. By performing Gaussian fitting of

the thermal neutron peaks and employing a quadratic polynomial to deduce the gamma ray background, the percentage of gamma rays within the range of three times the standard deviation (sigma) is obtained. For the thermal neutron peak, the percentage of gamma rays in Ce^{3+}-doped Li glass is approximately 13.8%, while in the GS20 glass sample the percentage of gamma rays is approximately 24.1%. The Ce^{3+}-doped Li glass has a lower misclassification rate for neutrons than the GS20 glass sample, indicating better neutron/γ discrimination performance.

As shown in Table 1, the physical and scintillation characteristics of Ce^{3+}-doped Li glass were compared with those of commercial GS20 glass and other types of Li glass. The scintillation decay times of the Ce^{3+}-doped Li glass were measured as 58 ns (fast component) and 415 ns (slow component). The fast component originates from the radiative recombination of Ce^{3+} ions acting as activators in the scintillator. Specifically, the 5d $\rightarrow$ 4f de-excitation transition of Ce^{3+} dominates the fast decay process.[43] This is attributed to the electric dipole-allowed nature of the 4f $\rightarrow$ 5d excitation transition in Ce^{3+}, which typically exhibits broadband emission and a short decay time.[44] In contrast, the slow component is likely associated with spontaneous emission processes involving transitions from higher-energy excited states to the final ground state.[45] Compared to the GS20 glass samples, Ce^{3+}-doped Li glass exhibits longer light attenuation components, likely attributed to the higher Ce^{3+} concentration. In addition, the Ce^{3+}-doped Li glass and the GS20 glass scintillator have low densities, which can effectively reduce sensitivity to γ-rays, benefiting neutron detection and achieving good neutron and gamma discrimination. Furthermore, the Ce^{3+}-doped Li glass exhibits a higher light yield for both gamma and neutron when compared to the GS20 glass sample. Therefore, it can be expected that the Ce^{3+}-doped Li glass can be a viable substitute for the GS20 glass scintillator, offering a potential alternative to ^{3}He gas.

Table 1. The key properties of Ce^{3+}-doped Li glass, GS20 glass and other types of Li glass.

Scintillator	ρ (g/cm^3)	Light yield (ph/MeV)	Energy resolution (662 keV)	Light yield (neutron)	Decay time (ns)
Li glass[a)]	2.9	$\sim$ 1600	31%	N/A	40, 2290
GS20	2.5	$\sim$ 4000[b)]	N/A	$\sim$ 6000[c)]	18, 57, 98[d)]
GS20 sample in this work	2.5	$\sim$ 2807	26.0%	$\sim$ 4861	49, 336
Ce^{3+}-doped Li glass in this work	2.47	$\sim$ 4770	14.5%	$\sim$ 7058	58, 415

[a)]Ref. [42], [b)]Ref. [33], [c)]Ref. [34], [d)]data obtained from Saint-Gobain product brochure.

4. Conclusion

In summary, the high Ce^{3+}-doped Li glasses were prepared using the high-temperature melting method, and the photoluminescence and scintillation properties were evaluated. Under UV and x-ray irradiation, emission peaks were observed at about 400 nm and 390 nm, which is due to the 5d–4f transition of Ce^{3+} ions. The pulse integration spectrum under ^{137}Cs γ-ray radiation exhibited a high light yield of 4770 ph/MeV and an energy resolution of 14.5%@662 keV. In addition, the neutron light yield of the Ce^{3+}-doped Li glass is about 7058 ph/neutron and the relative width of the thermal neutron peak is about 10.5% under Am–Be neutron source irradiation. The neutron yield of the Ce^{3+}-doped Li glass was found to be about 1.18 times that of commercial GS20 glass, and the number of gamma rays that might be wrongly identified as neutrons is about 13.8%. This is much better than the value of 24.1% for the GS20 glass sample, which indicates much better neutron/γ identification performance was achieved. The quenching factor (q) of the Ce^{3+}-doped Li glass is 0.31 for the neutron reaction, which is slightly lower than the 0.36 for the GS20 glass sample. In the future, the structure of the glass material and the relationship between structure and luminescence will be studied in detail. The formulation and process will continue to be optimized to improve the quenching factor of Li glass and further increase the content of 6Li to improve the neutron detection efficiency. The high Ce^{3+}-doped Li glass will be a low-cost and high-efficiency neutron scintillator, which is favorable for applications in large-area neutron imaging detectors.

Acknowledgments

Project supported by the National Key R&D Program of China (Grant No. 2023YFF0721700) and the National Natural Science Foundation of China (Grant No. 12475312).

References

[1] Cai X J, Yu Q, Huang C, Tang B, Zhou S H, Wang X H, Yue X P and Sun Z J 2023 *Chin. Phys. B* **32** 110701

[2] Yue X P, Zhu Z F, Tang B, Huang C, Yu Q, Chen S J, Wang X K, Hong X, Zhou S H, Cai X J, Yang H, Wan Z Y, Sun Z J and Liu Y T 2023 *Chin. Phys. B* **32** 090402

[3] Arkharov A M, Arkharov I A, Dolgopyatov D A and Bondarenko V L 2013 *Chem. Petrol. Eng.* **49** 41

[4] Zhou C, Melton A G, Burgett E, Hertel N and Ferguson I T 2019 *Sci. Rep.* **9** 17551

[5] Kumar S, Herzkamp M, Durini D, Nöldgen H and Waasen S V 2020 *Nucl. Instrum. Methods Phys. Res. Sec. A* **954** 161697

[6] Dosovitskiy G, Akimova O, Amelina A, S Belus, A Fedorov, Karpyuk P, Kozlov D, Mechinsky V, Mikhlin A, Retivov V, Smyslova V, Volkov P and Korzhik M 2020 *Rev. J. Chem.* **10** 1

[7] Cieślak M, Gamage K and Glover R 2019 *Crystals* **9** 480

[8] Britvich G I, Vasil'chenko V G, Gilitsky Y V, Chubenko A P, Kushnirenko A E, Mamidzhanyan E A, Pavluchenko V P, Pikalov V A, Romakhin V A, Soldatov A P, Sumaneev O V, Chernichenko S K, Shein I V and Shepetov A L 2005 *Nucl. Instrum. Methods Phys. Res. Sec. A* **550** 343

[9] Nguyen L Q, Gabella G, Goldblum B L, Laplace T A, Carlson J S, Brubaker E and Feng P L 2021 *Nucl. Instrum. Methods Phys. Res. Sec. A* **988** 164898

[10] Yuan D, Víllora E G, Kawaguchi N, Daisuke Nakauchi, Kato T, Yanagida T and Shimamura K 2022 *Jpn. J. Appl. Phys* **62** 010614

[11] Ruan J, Xu M, Chen L, Sun B, Liu B, Liu J, Zhang Z, He S, Zhao K and Ouyang X 2020 *Nucl. Instrum. Methods Phys. Res. Sec. A* **953** 163190

[12] Zaitseva N, Glenn A, Martínez H, Carman L, Iwona Pawełczak, Faust M and Payne S A 2013 *Nucl. Instrum. Methods Phys. Res. Sec. A* **729** 747

[13] Doan T C, Majety S, Grenadier S, Li J, Lin J Y and Jiang H X 2015 *Nucl. Instrum. Methods Phys. Res. Sec. A* **783** 121

[14] Song R, Yan X, Han J, Luo X, Ren F, Zhang Y, Han Z, Wen C, Zhang X, Chen L, Lin W, Qu G, Liu X, Leng Q, Zhu J, Qian S and Wang Z 2023 *IEEE Trans. Nucl. Sci.* **70** 2148

[15] Sykora G J, Mann S E, Mauri G, Schooneveld E M and Rhodes and Rhodes N J 2024 *Opt. Mater. X* **24** 100373

[16] Min S, Kang H, Seo B, Cheong J, Roh C and Hong S 2021 *Energies* **14** 7701

[17] Kojima T, Katagiri M, Tsutsui N, Imai K, Matsubayashi M and Sakasai K 2004 *Nucl. Instrum. Methods Phys. Res. Sec. A* **529** 325

[18] Syntfeld A, Moszynski M, Arlt R, Balcerzyk M, Kapusta M, Majorov M, Marcinkowski R, Schotanus P, Swoboda M and Wolski D 2005 *IEEE Trans. Nucl. Sci.* **52** 3151

[19] Gektin A V, Shiran N V and Voronova V V 1997 *IEEE Trans. Nucl. Sci.* **44** 857

[20] Song R Q, Han J F, Yan X Y, Luo X B, Ren F X, Han Z, Wen C, Zhang X, Zhang Y R, Chen L, Yi C Q, Qu G F, Liu X Q, Lin W P, Leng Q Z, Zhu J J, Qian S, Wang Z G, Tong Y F and Tang G 2023 *Nucl. Instrum. Methods Phys. Res. Sec. A* **1055** 168533

[21] Tong Y F, Wei Q H, Song R Q, Zheng Z, Ma L S, Hua Z H, Qian S and Qin L S 2023 *Opt. Mater.* **142** 114119

[22] Ren F X, Han J F, Song R Q, Qian S, Wei Q H, Tang G, Liu X Q, Qu G F, Zhang J X, Yi C Q, Chen Y M, Ren P P, Sun X Y, Cai H, Ban H Y, Wang Z L and Ren J 2024 *J. Instrum.* **19** P08025

[23] Yi C Q, Han J F, Song R Q, Yan X Y, Ren F X, Luo X B, Han Z, Wen C, Qu G F, Liu X Q, Lin W P, Wang P, Fan Y X, Qian S, Wang Z G, Tang G, Qin L S, Wang X and Liu J 2023 *Nucl. Instrum. Methods Phys. Res. Sec. A* **1055** 168561

[24] Kim C, Lee W, Melis A, Elmughrabi A, Lee K, Park C and Yeom J Y 2021 *Crystals* **11** 669

[25] Nikl M and Yoshikawa A 2015 *Adv. Opt. Mater.* **3** 463

[26] Tong Y F, Wei Q H, Shu C, Yin H, Zhang S Y, Zheng Z Q, Cai P Q, Liu Z G, Ma L S, Song R Q, Hua Z H, Qian S and Qin L S 2023 *J. Cryst.* **613** 127200

[27] Moore M E, Pavel Trtik, Lousteau J, Pugliese D, Brambilla G and Hayward J P 2019 *J. Lightwave Technol.* **37** 5699

[28] Katagiri M, K Sakasai, M Matsubayashi and Kojima T 2004 *Nucl. Instrum. Methods Phys. Res. Sec. A* **529** 317

[29] Stephan M, Zachau M, Gröting M, Karplak O, Eyert V, Mishra K C and Schmidt P C 2005 *J. Lumin.* **114** 255

[30] Nikl M, Bruza P, Panek D, Vrbova M, Mihokova E, Mares J A, Beitlerova A, Kawaguchi N, Fukuda K and Yoshikawa A 2013 *Appl. Phys. Lett.* **102** 161907

[31] Dorenbos P 2002 *Nucl. Instrum. Methods Phys. Res. Sec. A* **486** 208

[32] Struebing C, Chong J, Lee G, Zavala M, Erickson A, Ding Y, Wang C-L, Diawara Y, Engels R, Wagner B and Kang Z 2016 *Appl. Phys. Lett.* **108** 153106

[33] Kimura H, Shinozaki K, Okada G, Kawaguchi N and Yanagida T 2018 *J. Non. Cryst. Solids.* **508** 46

[34] Miyazaki K, Daisuke Nakauchi, Kato T, Kawaguchi N and Yanagida T 2023 *Opt. Mater.* **146** 114557

[35] Teng L M, Zhang W N, Chen W P, Cao J K, Sun X Y and Guo H 2020 *Cern. Int.* **46** 10718

[36] Sun X Y, Liu X J, Wu Y, Xiao Z, Chen Q, Wang W F and Yang Q M 2019 *Cern. Int.* **46** 4035

[37] Hua Z H, Qian S, Cai H, Du D J, Fan R R, Han J F, Hu C, Hu P, Liu S, Liu Y, Ma L S, Qin L S, Ren J, Song R Q, Sui Z X, Sun X L, Sun X Y, Tang G, Wang Z G, Wu Q, Yang D, Zheng L R and Zhu Y 2024 *Radiat. Detect. Technol. Methods* **8** 1107

[38] Bliss M, Craig R A and Reeder P L 1994 *Nucl. Instrum. Methods Phys. Res. Sec. A* **342** 357

[39] Bollinger L M, Thomas G N and Ginther R J 1962 *Nucl. Instrum. Methods Phys. Res. Sec. A* **17** 97

[40] Mesick K E, Coupland D D S and Stonehill L C 2017 *Nucl. Instrum. Methods Phys. Res. Sec. A* **841** 139

[41] Ferrulli F, M. Labalme and M. Silari 2022 *Nucl. Instrum. Methods Phys. Res. Sec. A* **1029** 166460

[42] Saha S, Ntarisa A V, Nguyen D Q, Luan N T, Vuong P Q, Kim H J, Intachai N, Kothan S and Kaewkhao J 2022 *Radiat. Phys. Chem.* **199** 110285

[43] Kamada K, Endo T, Tsutumi K, Yanagida T, Fujimoto Y, Fukabori A, Yoshikawa A, Pejchal J and Nikl M 2011 *Cryst. Growth. Des.* **11** 4484

[44] Liu J, Zhao X D, Xu Y S, Wu H D, Xu X H, Lu P, Zhang X H, Zhao X J, Xia M L, Tang J, Niu G D 2023 *Laser. Photonics. Rev.* **17** 2300006

[45] Kumar V and Luo Z 2021 *Photonics* **8** 71